LOW-VOLTAGE FED ENCODERLESS MOTOR DRIVE DEVOTED TO WHEELCHAIRS FOR A SUSTAINABLE MOBILITY

A. Lidozzi, V. Serrao, L. Solero, F. Crescimbini, A. Di Napoli
University of ROMA TRE, DIMI - Dept. of Mechanical and Industrial Engineering
Via della Vasca Navale 79 – 00146 Roma, Italy
lidozzi@ing.uniroma3.it, serrao@uniroma3.it

***Abstract* – This paper reports the results achieved through the development of a prototype of electric wheelchair having direct-drive motors being housed within the wheel rims and designed to achieve performance as required for such a particular 24 V battery-operated vehicle application. The main levels of innovation of the realized prototype are described: the design and construction of two twin AFPM wheel-motor drives; the design and modeling of controllers together with the regulators tuning; the design and realization of the power conversion section; the development of a back-EMF-based method in conjunction with Hall-effect sensors to estimate rotor speed and position. Then, EMC characterization of the electric wheelchair is presented.**

***Keywords* – Axial Flux Permanent Magnets Machine, EMC characterization, encoderless, low voltage inverter, vector control.**

ABBREVIATIONS LIST

AFPM	Axial Flux Permanent Magnet
DSP	Digital Signal Processor
EMC	Electromagnetic Compatibility
EMF	Electromotive Force
EMI	Electromagnetic Interference
EUT	Equipment Under Test
ITE	Information Technology Equipment
PCB	Printed Circuit Board
PDS	Power Drive System
PM	Permanent Magnet
PMSM	Permanent Magnet Synchronous Motor
SERF	Speed Estimator based on Rotor Frame
SVM	Space Vector Modulation

I. INTRODUCTION

This paper describes the development of a 24 V battery-operated prototype of electric wheelchair.

Two aspects give the main level of innovation of the realized prototype. Firstly it has been accomplished the replacement of standard (chopper-fed) dc motor drives a commercially available wheelchair chassis was early equipped with, by means of two twin AFPM (Axial-Flux Permanent Magnet) wheel-motor drives. To the purpose of improving the wheelchair performance, the use of a direct drive motor is desirable in order to eliminate the gearbox, enhance the wheelchair range of autonomy and make the wheelchair drive train cheaper, quieter and more reliable. The further aspect of innovation is the removal of unreliable and expensive rotor position sensors. The rotor position of direct-drive AFPM, to be used for traction purpose of the electric wheelchair, is estimated by using a back-EMF-based method in conjunction with three very low-cost integrated circuits based on the Hall-effect.

First project activities were finalized to design and construction of the mentioned two twin AFPM wheel-motor drives. In fact, slotless AFPM machines proved to be particularly suitable for low-speed high-torque applications and, as in comparison with other machine topologies they allow direct drive motor designs which result in higher lightness and compactness of the machine. The use of AFPM wheel motors in wheelchair traction drives allows substantial improvement of drives overall efficiency and reduction of power consumption thereby [1-3].

Other project activities were aimed to the design and modeling of controllers for the new AFPM drives for both steady state and dynamic behavior; regulators tuning is also carried out, as well complete control system implementation on DSP (Digital Signal Processor) board is accomplished. The particular motion requirements are the main constraints in controllers design in order to achieve smooth driving sensation and maneuverability at very low speed.

Fig. 1. Electric wheelchair equipped with proposed wheel motor drive prototypes.

The wheelchair power conversion section is accomplished by means of two MOSFET inverters, one for each motor drive; the whole structure includes the measures acquisition system (temperature, voltage and current sensors) and the power driving stage. The electric and mechanical layout was designed and realized in order to obtain a reliable and mechanically compact dc-ac converter.

In order to overcome disadvantages of using position sensors, which are required to time the sinusoidal current waveforms with the rotor position, a Speed Estimator based

Manuscript received on May 15, 2006; first revision on September 4, 2006; second revision on September 28, 2006. Recommended by the Editors of the Special Section José A. Pomilio and Andrés Ortiz Salazar.

on Rotor Frame machine model (SERF) has been implemented for the PMSM drives. Then, the rotor position estimation is achieved by means of a discrete integration of the estimated speed. Three Hall effect sensors are used to detect the rotor initial position [4-7] as well to reset the error on the rotor position estimation every 60 electrical degrees. The electric wheelchair equipped with the proposed wheel motor drive prototypes is shown in Figure 1.

II. WHEEL MOTOR PROTOTYPE

Due to their modes of operation, electric wheelchairs have motion requirements which somewhat differ from those ones of others road vehicles, namely lower rating speed (e.g. maximum speed of 10÷15 km/h on a flat road) and extremely higher peak torque in the form of a pulse of short duration (e.g. a single-shot peak torque of 6÷8 times the average torque along few decades of seconds). Such motion requirements severely constrain the design of a direct drive motor in terms of machine thermal behavior; as the need for very high overload capability together with a relatively low rotational speed of the motor require both operation with low power loss and effective cooling of the machine parts.

Hence, selection of the most suitable direct drive motor topology for the wheelchair application is not a straightforward process, since the motor design must allow the achievement of ill-matched requirements such as high both compactness and efficiency. Electrical machines with PM rotor excitation allow motor designs with the highest torque-to-mass ratio and offer the merit of operation with the lowest power loss. In fact, PM machines have no rotor losses, and for a given output torque the I^2R loss is significantly lower if compared with that one of machine topologies which use ac excitation (i.e. either the induction or reluctance machine topology) [8-10]. In the PM machines power losses are only found in the machine stator and this allows easy removal of heating by means of a suitable arrangement of heat dispersal paths.

In comparison with machines having the winding placed in slots, and thereby affected by significant power loss in the teeth of the iron core, the slotless arrangement of the machine winding further improves the machine efficiency, as the iron losses are minimized and found practically negligible in the low speed applications.

Due to both a disc-shaped machine structure and the advantageous characteristics as mentioned above, the AFPM topology was selected for the wheel motors to be used in the newly-conceived wheelchair prototype. As the novel gearless drive was intended to replace a standard dc motor-gear drive train the available wheelchair chassis was early equipped with, design specification for the two twin AFPM wheel motors was set in order to get overall drive performance same as those of a standard wheelchair drive. However the target efficiency was set as high as one could expect from using a conventional high-speed motor drive having same rating power.

An optimization procedure for the motor design has been applied on the basis of the specifications of Table I. The chosen optimization procedure maximizes the motor torque/weight ratio as a function of the ratio between the stator inner radius and the stator outer radius. The motor design which emerged as the most favorable of those meeting the specification is described by the leading quantities given in Table II.

TABLE I
Motor Design Specification

Cruising speed [km/h]	10
Rating power on each wheel [W]	200
Wheel diameter with tire under load [mm]	400
Peak torque on each wheel [N-m]	> 80
Efficiency @ rating condition	> 85%

TABLE II
Design Characteristics of Wheelchair Direct-Drive Motors

Number of poles	16
Rating power [W]	200
Nominal speed [rev/min]	136
Continuous torque [N-m]	14
Peak torque [N-m]	84
Phase peak emf @ nominal speed [V]	8.7
Phase rms current @ rated torque [A]	11
Efficiency @ rating power	86%
Number of phases	3
Number of coils per phase	16
Number of turns per coil	8
Conductor dimensions [mm x mm]	3.12 x 1.1
Phase resistance @ working temperature [mΩ]	90.5
Stator core outer diameter [mm]	260
Stator core inner diameter [mm]	180
Stator core axial thickness [mm]	7
Thickness of toroidal core strip iron [mm]	0.3
Thickness of rotor discs [mm]	6
Magnet material	Nd-Fe-B
Magnet dimensions [mm x mm]	40 x 30
Magnet thickness [mm]	6
Airgap peak flux density [T]	0.62
Machine overall axial length [mm]	55
Total mass of active materials [kg]	6.9

As the ac supply of the motor is obtained through a 24 V battery fed inverter, no particular frequency of the machine EMF is demanded. Therefore, high number of poles was chosen to give lightweight rotor and stator core. After consideration of many alternatives, a 16 poles machine arrangement was chosen and, at the wheelchair cruising speed of 10 km/h, this leads to a nominal frequency of 18 Hz. Due to the restriction imposed by the 400 mm wheel diameter, the outer diameter of the machine stator core had to be limited to 260 mm. As a compromise between maximizing the machine torque-to-mass ratio and achieving the required torque performance, the inner diameter of the stator core was set at 180 mm. The machine three-phase winding is accomplished by means of 1 coil per pole and per phase. Each coil consists of 8 turns being arranged in a single layer. To this purpose a 3.12 mm x 1.1 mm rectangular cross-section conductor is wound around the toroidal core with its 1.1 mm dimension being facing the airgap flux in order to minimize the eddy-current power loss in the winding. Magnet thickness of 6 mm is used in order to get airgap peak flux density of 0.62 T. The overall axial length of the machine is 55 mm and the overall mass of active materials is less than 7 kg, including about 1.8 kg of magnets. The machine rated torque of 14 Nm is achieved with phase rms current of 11 A and at the rating power the machine exhibits efficiency slightly exceeding the target of 85%. The selected

wheel motor design allows transient peak torque of 84 N-m over 15 s, as required in case of wheelchair low-speed operation for either getting over side-walk steps or climbing through 30% steep slopes.

Design of the complete wheel motor drive included the design of an original wheel rim for housing both the traction motor and the electromagnetic brake. Further to that, an unusual mechanical arrangement had to be conceived in order to provide a path for both power and signal (i.e. Hall-effect sensors) cables within the wheel hub. A shell-like wheel rim provides the required IP55 protection for the motor and it is used for housing the wheel tire.

Construction of the machine active parts includes manufacturing the toroidal stator and the two PM rotor discs as described in the following. The winding coils are mounted on a slotless toroidal core and then connected among them to achieve a three-phase winding arrangement. Thermocouples are also included in selected places within the winding for monitoring of the winding temperature during machine operation. The stator construction is completed by encapsulating the cored winding with epoxy resin which has the high thermal conductivity required for the dispersal of the stator power loss.

Extensive experimental test campaign was carried out in order to evaluate the wheel-motor drive performance and possibly assess the battery energy saving resulting from the use of a gearless drive arrangement instead of the standard dc motor drive the wheelchair chassis was early equipped with. Testing was accomplished by arranging an experimental rig including a test bench for electric traction drives being suitably equipped with a 4-channels power meter and both torque and speed transducers. The test bench is formed by an induction machine being connected to the power grid through a front-end inverter.

At the beginning of the test campaign, the standard wheelchair drive train including chopper-fed dc motor and speed reduction gear was tested in order to experimentally evaluate its performance over a wide range of torque and speed. Figure 2 shows efficiency curves (dashed line) resulting from test data achieved for the standard wheelchair drive train being operated at several speeds and power output up to 400 W. It clearly appears that at any operating condition the efficiency of the standard wheelchair drive is well below 60% and such a very poor efficiency is mainly attributed to the significant loss of power occurring in the reduction gear.

To the goal of evaluating the improvements resulting from the use of the newly-conceived direct-drive propulsion system, tests same as those early conducted on the standard wheelchair drive were carried out on one of the AFPM wheel motor drive. Efficiency curves resulting from test data collected for the AFPM drive are also shown in Figure 2 (continuous line). From the comparison with the efficiency curves of the standard wheelchair drive it is evident that over the entire range of power the wheelchair drive is expected to operate the AFPM wheel-motor drive offers superior performance in terms of energy conversion efficiency. In particular, it is found that at the 200 W rating power of the wheelchair drive the AFPM wheel motor arrangement is capable to deliver the required torque with less than half the power loss occurring in the standard wheelchair drive, thereby allowing substantially better utilization of the energy stored in the onboard battery and significant increase of the vehicle range of autonomy.

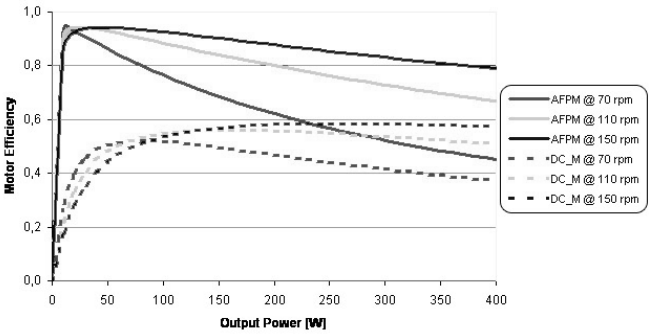

Fig. 2. Comparison of wheelchair motor drive efficiency: AFPM wheel motor drive; DC-M conventional drive.

III. INVERTER DESIGN

The investigated traction drive has the peculiarity of low-voltage power supply and it is characterized by high over-torque – and then high over current - mode of operation, thus suitable solutions have to be adopted to reduce voltage drops and to supply the drives with the potential maximum voltage. To this purpose the AFPM motors are fed by MOSFET inverters having low voltage drops and operating at 30 kHz switching frequency. The high difference between values of the switching frequency and the motor EMF rated frequency assures a good sinusoidal shape for the motor phase currents thus minimizing any audible motors noise.

In particular, the wheelchair is a 24 V battery-operated vehicle having two twin direct-drive AFPM wheel-motors fed by two inverters we have designed and realized on purpose. Every power section (PM motor drive) is made up of a 6-pack module by IXYS based on MOSFET technology with a very low (2.3 mΩ) static drain source on resistance ($R_{DS(on)}$), a drain source breakdown voltage (V_{DSS}) of 75 V and a continuous drain current (I_D) of 200 A (at case temperature of 80 ^oC). The total DC link capacitance (two paralleled capacitors) is 4700 μF. An experimental test rig which includes a programmable dc power source (200V-100A maximum) and the proposed traction motor is used to test the inverters. A 4-channels power meter is used to measure power and efficiency while the traction motor is loaded at different operating conditions by means of the test bench. Temperatures of motor winding and power electronic module case have been monitored during test execution, the found results assure the comfort for the wheelchair users is not affected by any temperature effect.

In Table III the inverter efficiency (η) is shown for different modulation indexes (M) and for peak current values (rated and overload). In Figure 3 a single wheelchair inverter is shown. The whole structure includes the measures acquisition system (temperature, voltage and current sensors) and power driving stage.

The electric and mechanical layout was designed and realized in order to obtain a reliable and mechanically compact module; a lot of care was spent to optimize the connections of both inverter power and control pins with the

rest of the system. In particular, gate signal pins are connected through a suitable PCB (Printed Circuit Board) directly soldered on the power module, whereas properly designed bus-bars (multiple laminated copper layers insulated by dielectric films) system was considered for the power connections in order to reduce stray inductances and eddy current losses.

TABLE III
Inverters efficiency

M	Operating conditions	η
0.6	Rated Current (16A)	90,2%
	Overload Current (91A)	87,3%
0.9	Rated Current (16A)	94,2%
	Overload Current (91A)	91,8%

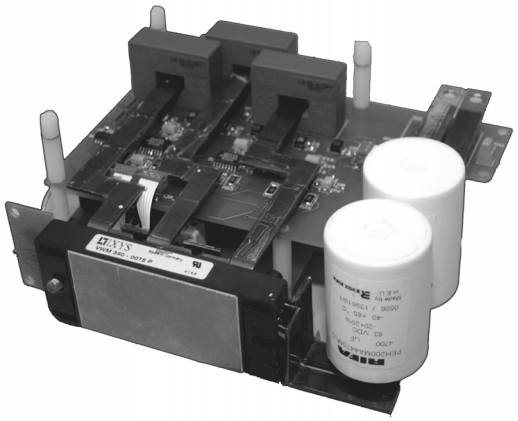

Fig. 3. Wheelchair motor drive inverter (bottom view).

Once the measures acquisition and control PCBs were realized, the whole structure, including the forced-air cooling system (heat sink and fan), was assembled into an aluminum suitable case to be located beneath the wheelchair seat. The twin inverters are illustrated in Figure 4 before final assembling of heat sink and fans.

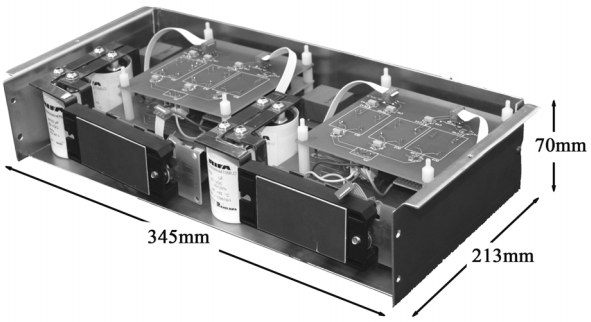

Fig. 4. Wheelchair inverters assembly (top view).

IV. CONTROLLERS DESIGN

A field oriented control technique is chosen, in which the *dq* reference frame is fixed with the rotor flux position. The control loops' design has been investigated by means of Matlab-Simulink models, where quantization of measures and control delays have been taken in consideration as well as true calculus mode adopted on DSP and control loop delays have been included. In order to tune the control of PMSM machine it is essential to derive the transfer function of the entire closed loop system. To simplify the design procedure, the speed and torque controllers are based on the assumption that the d-axis current is zero. This condition allows the system to be linear and independent of the cross coupling between the d and q-axes in the plant equation. Thus the entire system can be folded on q-axis and the linear system design methods can be applied.

In Figure 5 AFPM drive response is shown at speed reference step variation. For speed loop regulator performance, the comparison with a more complex (2-zeros/3-poles) controller has been carried out; in this case, however, PI regulator shows very close performances to the more complex regulator. As a consequence, the easier implementation of the PI controller led to its selection for the speed loop. Concerning the torque loop regulator, the comparison with a less heavy PI voltage regulator expression, from DSP calculus point of view, has been achieved; results in Figure 6 show higher performance of the 1-zero/2-poles designed controller as far as steady state error is considered.

Butterworth II order low-pass filters have been used in order to cancel the ripples at switching frequency in the measured currents i_{ABC}. The cut-off filter frequency has been set to 3 kHz and the Tustin method has been used to implement in discrete form the controller transfer functions with sampling time set to 400 μs. ADSP-21992 fixed point 16-bits DSP from Analog Devices has been used to implement the designed controllers for each traction drive.

Both drives are speed controlled and the driver sets the speed of both motors according to the position of a joystick. No problems are experimented in curve as the suitable differential speed is commanded in order to follow the desired path.

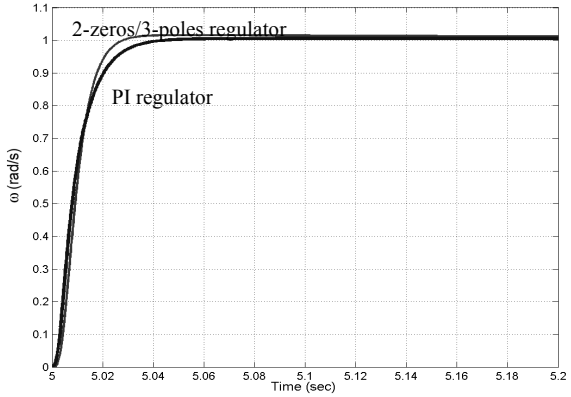

Fig. 5. AFPM drive response at reference speed step variation: 2-zeros/3-poles regulator, PI regulator.

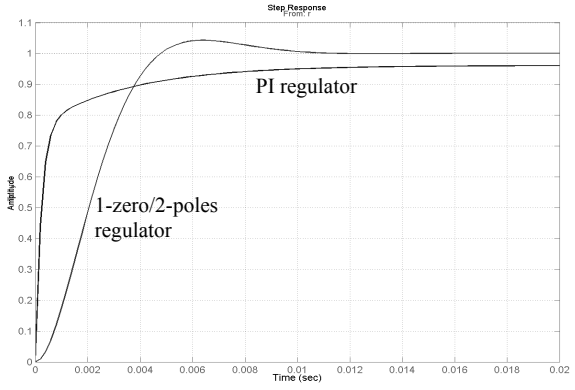

Fig. 6. Torque loop step response: 1-zero/2-poles regulator, PI regulator.

V. SPEED ESTIMATOR BASED ON ROTOR FRAME MACHINE MODEL (SERF)

The speed estimator based on the rotor frame machine model (SERF) is achieved by using the mathematical expressions of the PMSM model on d-q axes, which are stated in (1)

$$\begin{aligned} v_q &= R_s \cdot i_q + \frac{d\lambda_q}{dt} + p\omega_M \cdot \lambda_d \\ v_d &= R_s \cdot i_d + \frac{d\lambda_d}{dt} - p\omega_M \cdot \lambda_q \end{aligned} \quad (1)$$

where $\lambda_d = L_d \cdot i_d + \lambda_{af}$, $\lambda_q = L_q \cdot i_q$, R_s and $L_{d\text{-}q}$ are respectively the machine phase resistance and inductance on d-q axes, λ_{af} is the total rotor flux, ω_M is the mechanical rotational speed, and p is the number of poles pairs.

As a consequence, the electrical speed $\omega_e=p\omega_M$ and the rotor electrical position θ_e are calculated by means of respectively (2) and (3) where T_s is the sampling time used for executing the SERF algorithm, $L_s=L_d=L_q$, and $R_s=R_d=R_q$

$$\omega_{e(i)} = \left[v_{q(i)} - R_s i_{q(i)} - L_s \cdot \left(\frac{i_{q(i)} - i_{q(i-1)}}{T_s} \right) \right] \cdot \frac{1}{\lambda_{af} + L_s i_{d(i)}} \quad (2)$$

$$\vartheta_{e(i)} = \vartheta_{e(i-1)} + \frac{\omega_{e(i)} + \omega_{e(i-1)}}{2} \cdot T_s \quad (3)$$

The control algorithm includes acquisition of Hall effect sensor signals and motor phase currents, abc/dq axes transformation, speed loop and torque loop regulators, SVM switching strategy, as well machine rotor speed and position estimation. The three Hall-effect sensors are suitable positioned in the machine stator in order to provide 60 electrical degrees resolution in rotor position sensing, then the SERF error of the rotor position estimation is reset every time the rotor's magnetic axes enters a new 60° sector that is univocally identified by means of the three Hall-effect sensors' binary code.

Block diagram for each one of the wheelchair AFPM drives is shown in Figure 7, where d-q voltages in (1) are calculated from measured inverter output line-to-line voltages by means of abc/dq transformation. However, both simulations and experimental results show that the SERF algorithm required values for d-q voltages can be directly achieved from d-q reference voltages calculated in the torque loop controller when voltage drops across the inverter are taken into account, without any reduction of accuracy in speed estimation and with the advantage of two voltage sensors saving.

VI. START-UP AND NEAR-ZERO SPEED OPERATION

PWM-SVM technique [11] has been implemented together with the field oriented control with the purpose to extend as much as possible the linear modulation range. It should be noticed that SVM techniques, which are based on vector representation of the inverter, divide the plane in 6 sectors identified by a binary code in the same way the Hall effect sensors provide 60 electrical degree resolution in the rotor position sensing.

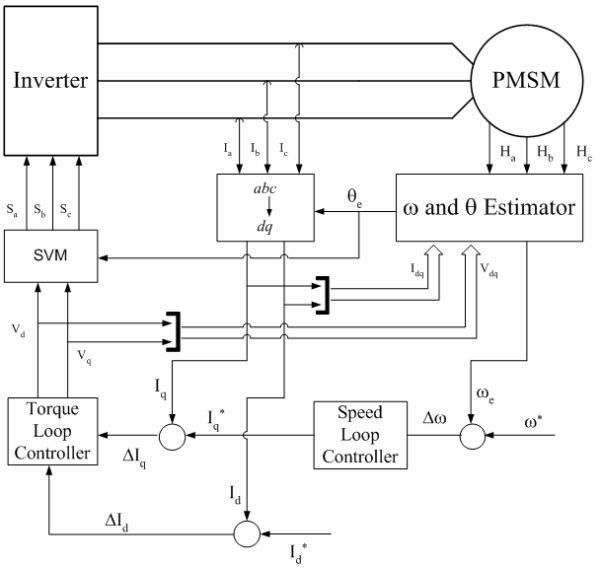

Fig. 7. Block diagram of PMSM drive with proposed SERF algorithm.

At the very first start, absolute position is obtained from the three Hall-effect sensors being faced to one motor pole pair; in this case, as shown in Figure 8, the rotor's magnetic axes position is assumed at the half of the 60° electrical sector identified by means of the sensors' binary code. As a consequence, the drive is able to start in sinusoidal operation at a torque which is in the range of 86.6%-100% of the maximum torque, in fact the maximum error in the initial position detection is 30 electrical degrees and it is reset to zero at the very first transition of any of the three Hall-effect sensors. Being the sampling time in the control algorithm set at 400 μs, the new values of electrical speed $\omega_{e(i)}$ and position $\theta_{e(i)}$ are achieved every 400 μs.

First simulations and also experimental results evidenced that, when the d-q voltage values required for the SERF algorithm are directly achieved from d-q reference voltages calculated in the torque loop controller, a steady state overestimation error is present in the speed. It has been observed that the steady state error is due to the voltage drop in the inverter power switches and diodes, and it can be considered somewhat proportional to the load current. Thus, (2) has been changed in (4) where the term $R_{av} \cdot i_{q(i)}$ takes fairly into account the voltage drop in the power inverter, and R_{av} is calculated as the average value of the equivalent resistances of MOSFETS and diodes.

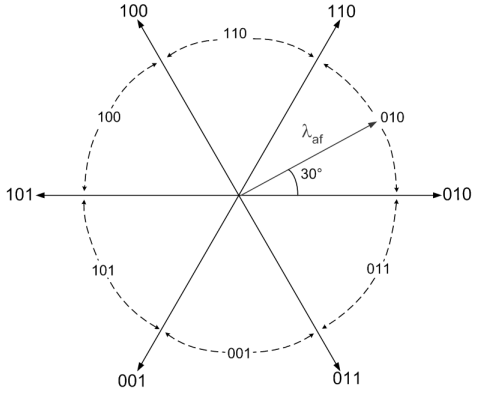

Fig. 8. Rotor's magnetic axes position at very first start-up.

$$\omega_{e(i)} = \left[v_{q(i)} - R_{av} i_{q(i)} - R_s i_{q(i)} - L_s \cdot \left(\frac{i_{q(i)} - i_{q(i-1)}}{T_s} \right) \right] \cdot \frac{1}{\lambda_{af} + L_s i_{d(i)}} \quad (4)$$

VII. SIMULATION RESULTS

The phase currents of the PMSM are shown in Figure 9 for the first 0.8 s of the simulation; at start-up one of the phase current is equal to zero because rotor's magnetic axes position is assumed at the half of the 60° electrical sector identified by means of the Hall sensors' binary code, at 0.13 s the rotor's magnetic axes enters the first new 60° sector and the initial error on the rotor position estimation is reset. From this point on the phase currents are correctly timed with the respective EMF waveforms.

Figure 10 shows the comparison between the estimated position and the actual position of the PMSM rotor, these simulation results confirm the good estimation achieved with SERF algorithm and the correct assumption for the start-up of the machine. It is clearly shown the assumed 30° (0.523 rad) error in the initial rotor position, is then reset at 0.13 s.

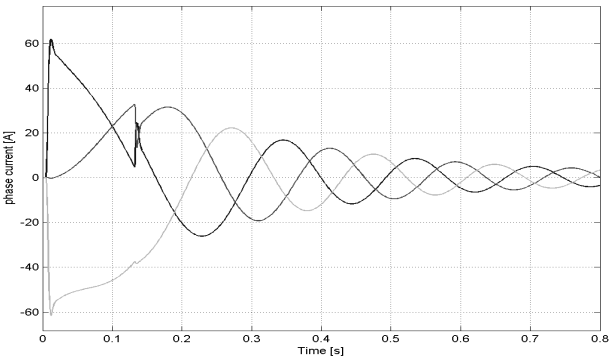

Fig. 9. PMSM phase currents at start-up.

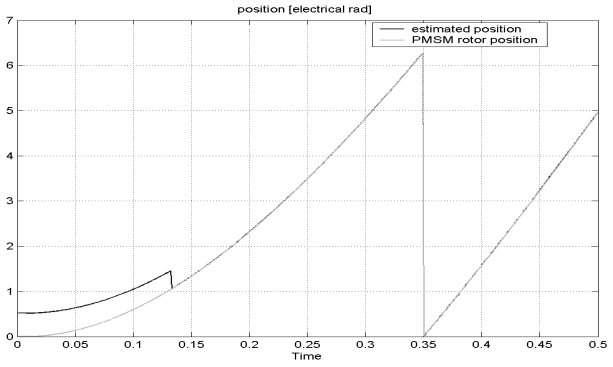

Fig. 10. Simulation result: estimated and actual rotor position at start-up.

VIII. EXPERIMENTAL RESULTS

Extensive experimental test campaign has been carried out for the prototypal AFPM motor drive using the SERF algorithm in the control loop.

First experimental tests, on the prototypal AFPM motor drive using the SERF algorithm in the control loop, have been devoted to prove the effectiveness of the proposed estimation algorithm at steady state modes of operation. For respectively positive and negative rotational speed, Figures 11a and 11b show estimated speed, actual speed, current of phase A and estimated position when the mechanical reference speed is 5 rad/s and the rated continuous load torque is applied. Throughout the experimental activity, for oscilloscope visualization purposes, the motor phase currents are measured by means of 200 kHz bandwidth current probes, and all the speed signals are achieved through a 12-bits D/A converter.

The experimental test evidences the absolutely negligible error in the speed estimation with respect to the actual speed, which is measured by means of a 1024 pulses incremental encoder. The Hall effect sensor of stator phase A, which is also shown, confirms both the correctness of the rotor position estimation and the alignment of the phase current with respect the machine phase EMF. Same waveforms are shown in Figure 12, where the speed reference oscillates at about 4Hz between 1rad/s and 3rad/s. The achieved results prove that the proposed SERF algorithm provides accurate estimation of the rotational speed even in transient modes of operation at very low speed.

The performance of the proposed speed estimation algorithm has been experimentally investigated also at start-up of the AFPM drive, in Figure 13 is shown the behavior of the electric drive using the SERF algorithm at reference speed variation respectively from 0 to 6 rad/s. Performances of the drive are very similar to the results observed during simulations, at start-up the current in phase A is equal to zero because rotor's magnetic axes position is assumed at the half of the 60° electrical sector identified by means of the Hall sensors' binary code, when the rotor's magnetic axes enters the first new 60° sector the initial error on the rotor position estimation is reset and each phase current is correctly timed with the respective EMF waveform.

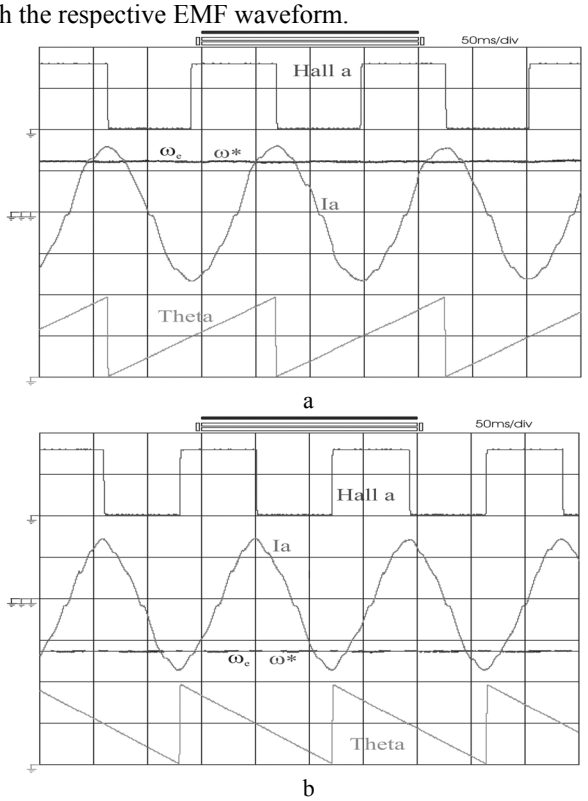

Fig. 11. Experimental results at 5rad/s: actual speed (4rad·s^{-1}/div), estimated speed (4rad·s^{-1}/div), phase current (10A/div), estimated position (π rad/div), Hall effect sensor; a) positive rotational speed, b) negative rotational speed.

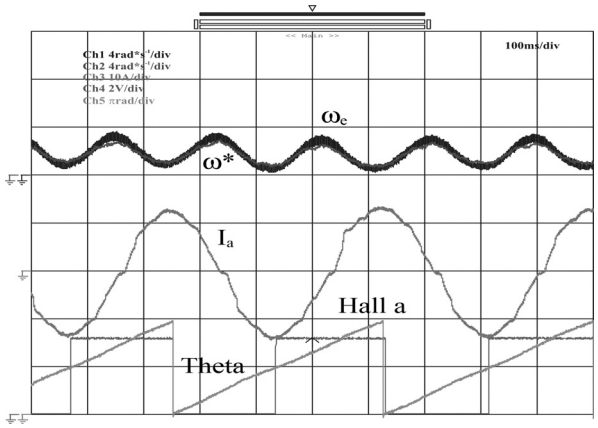

Fig. 12. Experimental results at 1-3rad/s: actual speed, estimated speed, phase current, estimated position, Hall effect sensor.

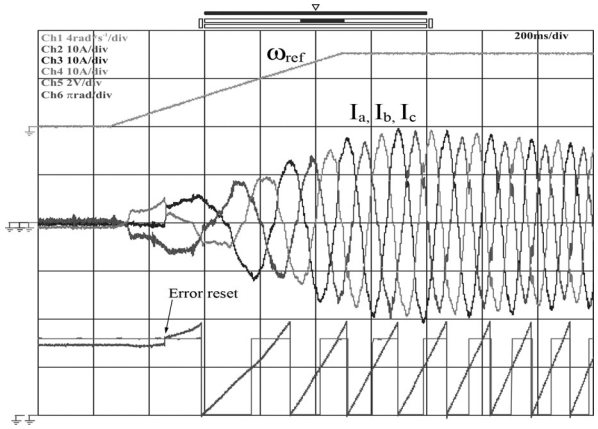

Fig. 13. Experimental results 0-6rad/s: currents of stator phase A, B, C, reference speed, rotor estimated position, Hall effect sensor.

IX. EMI CHARACTERIZATION

Electrically powered wheelchairs, as every electric and electronic device, should operate without introducing significant electromagnetic disturbances to the environment and without significant degradation of operational performance in the presence of electromagnetic disturbances that can be expected in normal use. Wheelchairs can be expected to operate in traffic areas and therefore should be immune to radio frequency fields from fixed and mobile communications equipment, as well as from other sources of electromagnetic disturbance. Injury could occur in the event of unintentional movement or change in direction of a wheelchair.

Today vehicles are equipped with sensitive communication and control systems, making the issue of EMI radiated from the power cables very important. Furthermore, with the recent advent of adjustable speed drives, new sources and mechanisms of producing common mode and differential mode currents due to inverter generated common mode voltages have been identified. Apart from voltages and currents generated by the motor itself, new effects have been observed when the motor is supplied from an SVM inverter, especially when the switching frequency increases.

An extensive and accurate emission (both radiated and conducted) testing campaign in a semi-anechoic chamber has been carried out to obtain the wheelchair EMC characterization. In particular, the influence and the interactions between the main subcomponents of the wheelchair PDS (Power Drive System) such as power electronics, driving circuits and control circuits have been evaluated. Besides, the investigation of alternative test procedures has been accomplished to estimate the wheelchair EMC performance even during actual modes of operation (start-up, acceleration, turning, deceleration and braking).

The main reference standard for EMC testing of such a vehicle is the international standard ISO 7176: 2003 – Part 21 "Wheelchairs – Requirements and test methods for electromagnetic compatibility of electrically powered wheelchairs and motorized scooters" [12]. It specifies requirements and test methods for wheelchairs to minimize the risk connected with reasonably foreseeable electromagnetic interference and electrostatic discharge. Suggestions are also added to minimize the risk of producing electromagnetic fields which could impair the operation of other devices or equipment in the wheelchair's usual environment. This standard, as far as it concerns the emission testing (both conducted and radiated), recalls the CISPR 11 standard (or the European corresponding CEI EN 55011) [13] "Industrial, scientific and medical RF equipment. Electromagnetic disturbance characteristics – Limits and methods of measurements". For the measuring equipment and methods the relevant standards are the CISPR 16 (or CEI EN 55016) "Specifications for radio disturbance and immunity measuring apparatus and methods" and the CISPR 22 (or CEI EN 55022) "Limits and methods of measurement of radio disturbance characteristics of information technology equipment (ITE)".

In particular, the wheelchair under test is classified as category A (wheelchairs with electronic differential steering and electronic brake control) and shall meet the requirements of the Group 1 - Class B conducted and radiated emissions limits of CEI EN 55011; then, emissions must be measured on a test site.

A test site for type testing shall allow emissions from the EUT (Equipment Under Test) to be distinguished from ambient noise; also, a controlled environment is required to assure reliability and repeatability of the performed measures and obtained results. For conducted emission testing we have used a shielded room as test site, whereas radiated emission testing has been performed in a semi-anechoic chamber, both sites being located in the PED (Power Electronics & Drives) section of the Mechanical and Industrial Laboratory of the University "Roma Tre".

In order to separate the different contributions to the wheelchair radiated emissions we have first switched on the control section (DSP) without modulation. As the DSP begins to modulate and it provides the duty cycles for the power section switches, the radiated emissions from the EUT change as shown in Figure 14. Some peaks increase their amplitude and spread out in frequency but still remaining centered at the same frequencies (multiples and submultiples of the DSP core clock rate of 160 MHz) and maintaining their emission levels under the standard limits. In this case the inverters feeding the wheelchair wheel-motors are driven by a classic SVM modulation operating at a switching frequency of 30 kHz.

Then, the power section (inverters, drive circuits and measures acquisition circuitry) has been switched on but still maintaining the wheelchair motionless. In this condition there were detected no differences in the EUT emission levels with respect to the previous test.

The last step in this experimental activity was the analysis of the wheelchair emissions also during actual modes of operation (start-up, acceleration, turning, deceleration and braking). Even if this kind of test is only partially included in the reference standards, we have retained it very relevant in order to obtain a complete and accurate EMC performance evaluation of our EUT. The final results are shown in Figure 15. It is noticeable that, during transients, the radiated emissions from the wheelchair during repeated manoeuvres (receiver being positioned in max hold mode) increase their amplitude with respect to the previous case. However, it must be remarked there is not yet any reference standard relevant to transient tests at the moment.

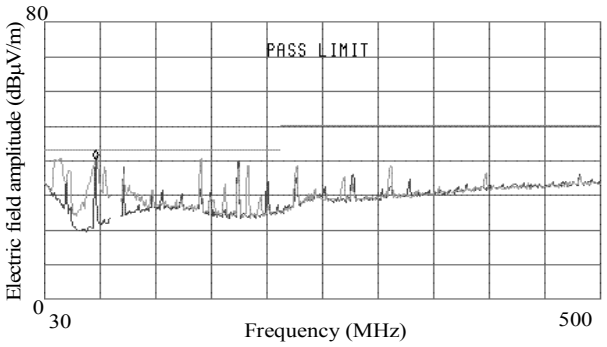

Fig. 14. Radiated emissions related to only DSP switched on and DSP modulating.

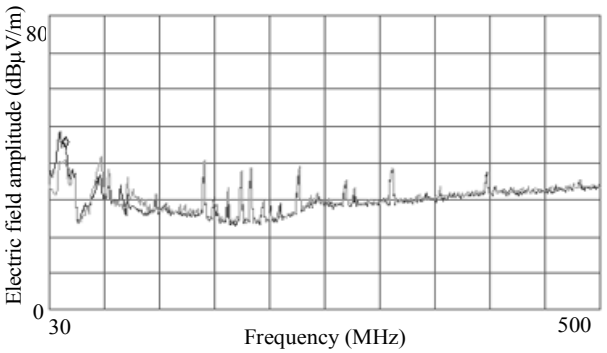

Fig. 15. Comparison between radiated emission levels during actual modes of operation and in steady state.

X. CONCLUSION

In this paper the results achieved through the development of a prototype of electric wheelchair are described. The presented vehicle main features (wheel motor drive, control technique with low resolution sensors, SERF estimator) make the overall system a very performing one. The wheelchair high range of autonomy makes it suitable for outdoors moving (in urban environment), while its maneuverability makes it an ideal vehicle for moving in indoor spaces with the presence of obstacles. The high range autonomy is the direct consequence of the high efficiency (in relation to such a particular application) of the proposed system which is addressed in sections II and III. The maneuverability is the direct consequence of the control system and it is addressed in section IV.

REFERENCES

[1] F. Caricchi, F. Crescimbini, A. Di Napoli, O. Honorati, E. Santini - Compact Wheel Direct Drive for EV's" - *IEEE Industry Applications Magazine*, November/December 1996, Vol. 2, No. 6, pp. 25-32.

[2] C. C. Chan, "Axial-Field Electrical Machines – Design and Applications," *IEEE Trans. on Energy Conversion*, vol. EC-2, n. 2, June 1987, pp. 294-300.

[3] R. Nilssen, S.E. Skaar, R. Lund, T. Skjellnes, S. Ovrebo, E. Lovli, "Design of a Permanent Magnet Synchronous Motor Integrated in the Wheel Rim on Wheelchairs", *Proc. of European Conference on Power Electronics and Applications 2005*, Sept. 2005, cd-rom.

[4] S. Morimoto, M. Sanada and Y. Takeda, "Sinusoidal Current Drive System of Permanent Magnet Synchronous Motor with Low Resolution Position Sensor", *Proc. of 1996 IEEE IAS Annual Meeting*, pp 9-13, Oct. 1996.

[5] J. Bu, L. Xu, T. Sebastian and B. Liu, "Near-Zero Speed Performance Enhancement of PM Synchronous Machines Assisted by Low Cost Hall Effect Sensors", *Proc. of IEEE APEC'98*, pp 68-74, Feb. 1998.

[6] S. Morimoto, M. Sanada and Y. Takeda, "High Performance Current- Sensorless Drive for PMSM and SynRM with only Low Resolution Position Sensor", *IEEE Transactions on Industry Applications*, Vol.39, N°3, pp 792-801 May/June 2003.

[7] F. Giulii Capponi, G. De Donato, L. Del Ferraro, "Brushless AC Drive Using An Axial Flux Synchronous Motor With Low Resolution Position Sensors", *Proc. of IEEE 35th Annual Power Electronics Specialists Conference, PESC'04*, cd-rom.

[8] E. Spooner, B.J. Chalmers, "TORUS - a slotless toroidal-stator, permanent magnet generator", *IEE Proceedings - part B*, 139, November 1992, pp. 497-506.

[9] F. Caricchi, F. Crescimbini, O. Honorati, "Low-Cost Compact Permanent Magnet Machine for Adjustable-Speed Pump Application", *IEEE Trans. on Industry Applications*, Vol. 34, No. 1, January/February 1998.

[10] P. Pillay, R. Krishnan, "Modeling, Simulation, and Analysis of Permanent-Magnet Motor Drives, Part I: The Permanent-Magnet Synchronous Motor Drive" *IEEE Trans. on Industry Applications*, vol. 25, no. 2, March/April 1989.

[11] G. Vitale, A. Di Napoli, F. Crescimbini, A. Lidozzi, L. Solero, "Combination of SVM Techniques for Electric Drives," *SPEEDAM 2004*, cd rom.

[12] "Wheelchairs – Requirements and test methods for electromagnetic compatibility of electrically powered wheelchairs and motorized scooters", *ISO 7176-21*, 1st ed, 2003.

[13] "Industrial, scientific and medical (ISM) radio-frequency equipment – Radio disturbance characteristics – Limits and methods of measurement", *CEI EN 55011* (and relative Amendments A1, A2), 2nd ed, 2003.

BIOGRAPHIES

Alessandro Lidozzi received the Electronic Engineering degree from the University of Rome “ROMA TRE,” Rome, Italy, in 2003. Since Nov. 2003 he has been a PhD Student with the Department of Mechanical and Industrial Engineering, University of “ROMA TRE”. His research interests are mainly focused in multi-converter based applications, dc-dc power converters modeling and control, and non-linear control of permanent magnet motor drives. Mr. Lidozzi is member of the IEEE Industrial Electronics Society. In 2004 he won a Student Award and a Travel Grant at ISIE – International Symposium on Industrial Electronics.

Vittoria Serrao received the Laurea degree in Electronics Engineering from the University of Rome “ROMA TRE”, Italy, in 2004. She is currently Ph.D. student with the Department of Mechanical and Industrial Engineering of the University of Rome “ROMA TRE”. Ms. Serrao main topics of interest are power electronics, control and interface PCBs design and related EMC issues.

Luca Solero received the Electrical Engineering degree from the University of Rome “La Sapienza,” Rome, Italy, in 1994. Since 1996 he has been with the Department of Mechanical and Industrial Engineering, University ROMA TRE where he currently is an Assistant Professor. During 2002 he was a Visiting Scholar at the Center for Power Electronics Systems (CPES), Virginia Polytechnic Institute and University, Blacksburg. His research interests include power converter topologies, permanent magnet motor drive and control systems design for unconventional applications such as electric and hybrid vehicle and renewable energy systems. Mr. Solero is a member of the IEEE Industry Applications, IEEE Power Electronics and IEEE Industrial Electronics Societies.

Fabio Crescimbini received the degree in Electrical Engineering and the Ph.D. degree both from the University of Rome "La Sapienza", Rome, in 1982 and 1987, respectively. From 1989 to 1998 he was with the University of Rome "La Sapienza", Department of Electrical Engineering, being there in charge as Director of the Electrical Machines and Drives Laboratory. In 1998 he joined the University ROMA TRE, Department of Mechanical and Industrial Engineering, where he currently is Full Professor of Electrical Machines and Drives. His research interests include newly-conceived permanent magnet machines and power converter topologies for unconventional applications such as electric vehicle motor drives and renewable energy generating systems. Prof. Crescimbini is an active member of both the IEEE Industry Applications Society (IAS) and the IEEE Vehicular Technology Society (VTS). Since 2001 he serves as member of the IEEE IAS Executive Board.

Augusto Di Napoli received the M. Sc degree in Electrical Engineering in 1969 from the University of Rome "La Sapienza", Rome. From 1970 to 1992 he was with the University of Rome "La Sapienza", Department of Electrical Engineering as Assistant Professor (1970), Associated Professor (1980) and then Full Professor of Electrical Drives (1986). In 1992 he joined the University ROMA TRE as Full Professor at the Department of Mechanical and Industrial Engineering; where, since 2002, he currently is the Head of the Department. His scientific interests include FEM analysis for electrical machines, control design and EMC analysis in electrical drives. Prof. Di Napoli is author of more than 90 papers published in international journals and in conferences proceedings.